NJC

PAPER

View Article Online
View Journal | View Issue

Cite this: *New J. Chem.*, 2017, 41, 2020

Synthesis, photophysical and nonlinear optical properties of a series of ball-type phthalocyanines in solution and thin films†

Njemuwa Nwaji, John Mack, Jonathan Britton and Tebello Nyokong*

Received 23rd November 2016,
Accepted 20th January 2017

DOI: 10.1039/c6nj03662g

rsc.li/njc

In this study, we report on the enhanced nonlinear optical properties of novel tetrakis-4-(hexadecane-1,2-dioxyl)-bis(phthalocyaninato zinc(II)) (**4**), tetrakis-4-(hexadecane-1,2-dioxyl)-bis(phthalocyaninato gallium chloride) (**5**) and tetrakis-4-(hexadecane-1,2-dioxyl)-bis(phthalocyaninato indium chloride) (**6**) both in solution and when embedded in polymer thin films. Complexes **5** and **6** bearing heavy atoms showed enhanced triplet quantum yield and nonlinear optical response. The nonlinear third-order susceptibility and second-order hyperpolarizability values are also reported. Time dependent density functional theory (TD-DFT) calculations were performed in order to explain the origin of the observed UV-vis and magnetic circular dichroism (MCD) spectra of the complexes.

Introduction

Over the last few decades there has been increasing interest in the design of optical limiters that can afford a measure of protection to optical sensors and the human eye from laser-induced damage. Good optical limiters strongly attenuate high incident light intensity or fluence, while exhibiting high transmittance at low values. The development of new materials with strong nonlinear optical (NLO) properties continues to attract considerable research interest.[1] The NLO and optical limiting (OL) properties of porphyrins and phthalocyanines have received considerable attention[2–6] due to their thermal stability and extensive delocalized π electron systems.[7,8] Optical limiting materials have been found to possess multiphoton absorption, reverse saturable absorption (RSA), nonlinear scattering, or nonlinear refraction as the dominant mechanisms responsible for their NLO behaviour.[9] The presence of an extended π electron conjugation system can result in a significant increase in the triplet excited state lifetime, which leads to improved RSA at 532 nm for nanosecond laser pulses.[10]

Ball-type phthalocyanines possess highly conjugated π-systems and their possible applications in electrochemistry and photovoltaic cells have been reported.[11] Apart from one literature report,[12] optical limiting properties of ball-type phthalocyanines have not received much attention. In this paper, the NLO behaviour of novel ball-type tetrakis-4-(hexadecane-1,2-dioxyl)-bis(phthalocyaninato zinc) (**4**), tetrakis-4-(hexadecane-1,2-dioxyl)-bis(phthalocyaninato gallium chloride) (**5**) and tetrakis-4-(hexadecane-1,2-dioxyl)-bis(phthalocyaninato indium chloride) (**6**) (Scheme 1) is reported. The incorporation of a heavy atom (Ga, In, and Zn) into the central cavity of a Pc macrocycle will increase intersystem crossing thereby leading to high population of the triplet state which is required for improved NLO behavior. Phthalocyanines containing more than one ring such as bis-phthalocyanines are known to show improved optical nonlinearities due to their expanded π electron system,[13] hence ball-type Pcs are expected to show improved NLO behaviour. In addition, the formation of a ball-type dimer should lead to significant changes in the optical and electronic properties of Pc complexes. Long alkoxyl side chains could result in symmetry distortion. Previous reports have shown the importance of asymmetry on the photophysical, photochemical and optical limiting (OL) properties of phthalocyanines.[14] The NLO behaviour of complexes **4–6** was studied in solution and when embedded in polymer thin films using polystyrene as the polymer. Casting of optically active compounds in the solid state is a practical means of enhancing the optical limiting properties of materials.[15]

Experimental

Materials

Polystyrene (M_w 192 000 g mol^{-1}), zinc acetate, gallium chloride, indium chloride, 4-nitrophthalonitrile (**2**), and 1,2-hexadecanediol (**1**) were obtained from Sigma Aldrich. Deuterated DMSO, tetrahydrofuran (THF), chloroform, 1,8-diazabicyclo[5.4.0]undec-7-ene (DBU), dimethyl formamide (DMF), methanol and dimethyl

Department of Chemistry, Rhodes University, Grahamstown 6140, South Africa. E-mail: t.nyokong@ru.ac.za; Fax: +27 46 6225109; Tel: +27 46 6038260

† Electronic supplementary information (ESI) available: NMR spectra and MALDI-TOF mass spectra, absorption and MCD spectra, B3LYP optimized geometries, biexponential decay curve of complex **6**, and table of theoretical calculations. See DOI: 10.1039/c6nj03662g

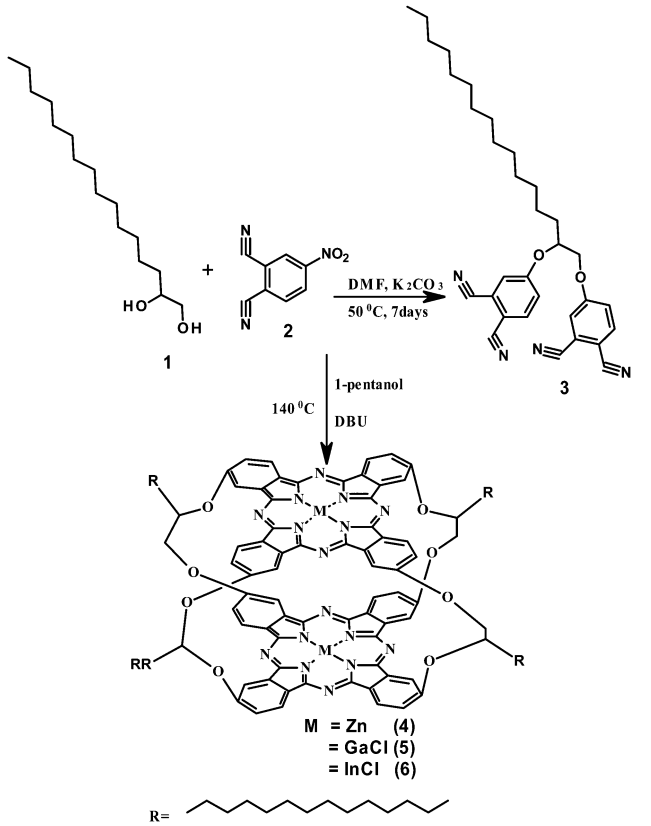

Scheme 1 Synthetic route for the preparation of complexes **4–6**.

sulphoxide (DMSO) were purchased from Merck. All solvents were of reagent grade. The purification processes were carried out by column chromatography on silica gel 60 (0.063–0.200 mm).

Equipment

Infrared (IR) spectra were recorded on a Bruker Alpha IR (100 FT-IR) spectrophotometer. ^{1}H NMR spectra were recorded on a Bruker AVANCE II 400 MHz NMR spectrometer using tetramethylsilane (TMS) as an internal reference. Elemental analyses were done using a Vario-Elementar Microcube ELIII, while mass spectra data were collected on a Bruker AutoFLEX III Smart-beam TOF/TOF mass spectrometer using a-cyano-4-hydrocinnamic acid as the matrix in the positive ion mode. Ground state electronic absorption spectra were recorded on a Shimadzu UV-2550 spectrophotometer. Fluorescence excitation and emission spectra were measured on a Varian Eclipse spectrofluorimeter using a 360–1100 nm filter. Fluorescence lifetimes were measured using a time correlated single photon counting setup (TCSPC) (FluoTime 300, Picoquant GmbH) with a diode laser (LDH-P-670, Picoquant_GmbH, 20 MHz repetition rate, 44 ps pulse width) as previously described.[16] Magnetic circular dichroism (MCD) spectra were measured using a Chirascan plus spectrodichrometer equipped with a 1 T (Tesla) permanent magnet by using both the parallel and antiparallel fields. The conventions of Piepho and Schatz are used to describe the sign of the MCD signal and the Faraday terms.[17] The triplet decay kinetics were determined using a laser flash photolysis system. The excitation pulses were produced by a tunable laser system consisting of a Nd:YAG laser (355 nm, 135 mJ/4–6 ns), pumping an optical parametric oscillator (OPO, 30 mJ/3–5 ns) with a 420 to 2300 nm (NT-342B, Ekspla) wavelength range as previously reported.[16] Triplet lifetimes were determined by the exponential fitting of the kinetic curves using the ORIGIN 6 Professional software. The absorbance value used for triplet state studies was kept at 1.5 and the solution was degassed by bubbling argon for 30 min prior to measurements.

All Z-scan analyses were performed using a frequency-doubled Nd:YAG laser (Quanta-Ray, 1.5 J/10 ns fwhm pulse duration) as the excitation source. The laser was operated in a near Gaussian transverse mode at 532 nm (second harmonic); details have been provided before.[18]

Syntheses

4-(Hexadecane-1,2-dioxyl)-bis(phthalonitrile) (3). A mixture of 1,2-hexadecanediol (**1**) (1.0 g, 3.86 mmol) and 4-nitrophthalonitrile (**2**) (1.34 g, 7.72 mmol) in dry DMF (20 mL) was stirred in a 100 mL round bottom flask at 50 °C under an inert atmosphere for 1 h. Dry K_2CO_3 (1.5 g, 10.5 mmol) was added in two equal portions at an interval of 6 h and the reaction was stirred undisturbed at ambient temperature for 7 days. The reaction mixture was poured into ice water and the precipitated product was filtered under reduced pressure. The light yellow precipitate was purified by column chromatography using THF/methanol (9 : 1) as the eluent to give a crystalline yellow solid. Yield: 0.95 g (41%), IR (ATR): ν (cm^{-1}): 2914 (Ar–CH), 2233 (C≡N), 1595 (C=N/C=C), 1248–1095 (C–O–C). ^{1}H NMR (300 MHz, DMSO) δ 8.26–8.05 (d, J = 8.1 Hz, 2H, Ar–H), 8.04 (d, J = 7.6 3.9 Hz, 2H, Ar–H), 7.55 (d, J = 7.5, 3.7 Hz, 2H, Ar–H), 4.28–4.20 (d, J = 9.2, 8.6 Hz, 3H, Aliph-H), 3.25 (t, J = 8.8, 8.6, 7.5 Hz, 2H, Aliph-H), 1.30–1.23 (m, 24H, long alkyl-H), 0.91 (s, 3H, long alkyl-H). MALDI TOF-MS: calculated: 510.30; found: 510.39 $[M + 1]^+$.

Tetrakis-4-(hexadecane-1,2-dioxyl)-bis(phthalocyaninato zinc(II)) (4). A mixture of zinc acetate (0.20 g, 1.4 mmol), 4-(hexadecane-1,2-dioxyl)-bis(phthalonitrile) (**3**, 0.25 g, 0.49 mmol), DBU (3 drops) and 1-pentanol (5 mL) was refluxed at 140 °C for 24 h under an argon atmosphere. Upon cooling, methanol was added and the precipitate was collected through centrifugation. The product was washed with methanol, ethanol and diethyl ether. The dark green product was further purified by column chromatography using THF and methanol (98 : 2) as the eluent to give a green product. The purified product was dried in an enclosed fume hood. Yield: 0.09 g (24%), IR (ATR): ν (cm^{-1}): 3017 (Ar–CH), 1613 (C=N/C=C), 1261–1138 (C–O–C). ^{1}H NMR (400 MHz, DMSO) δ 8.68 (dd, J = 8.8, 2.5 Hz, 1H, arom-H), 8.49 (d, J = 8.8 Hz, 2H, arom-H), 8.03 (m, 7H, arom-H), 7.51 (m, 8H, arom-H), 7.48 (m, 6H, arom-H), 5.12–4.98 (m, 3H, alkyl CH_2/CH), 4.48–4.18 (m, 8H, alkyl CH_2), 4.00 (m, 2H, alkyl CH_2), 1.78–1.75 (m, 7H, alkyl CH_2), 1.5–1.0 (m, 96H, alkyl-H) 0.80 (t, J = 6.9 Hz, 12H, alkyl CH_3). Anal: calc for $C_{128}H_{152}N_{16}O_8Zn_2$ C, 70.73; H, 7.05; N, 10.31. Found: C, 71.27; H, 6.88; N, 10.76. UV-vis., λ_{max}/nm (log ε): (THF), 682 (5.24), 617 (4.62), 349 (5.18). MALDI TOF-MS: calculated: 2173.52; found: 2173.81.

Tetrakis-4-(hexadecane-1,2-dioxyl)-bis(phthalocyaninato gallium(III) chloride) (5). Complex **5** was synthesised in the same

manner as **4** using gallium trichloride (0.3 g, 1.70 mmol), yield: 0.27 g (49%), IR (ATR): ν (cm^{-1}): 3003 (Ar–CH), 1607 (C═N/C═C), 1258–1115 (C–O–C). ^{1}H NMR (400 MHz, THF) δ 8.52 (dd, J = 8.1, 2.5 Hz, 1H, arom-H), 8.52 (d, J = 8.6 Hz, 2H, arom-H), 8.02 (m, 7H, arom-H), 7.53 (m, 8H, arom-H), 7.49 (m, 6H, arom-H), 5.03–4.85 (m, 3H, alkyl CH_2/CH), 4.52–4.25 (m, 9H, alkyl CH_2), 4.01 (m, 2H, alkyl CH_2), 1.78–1.75 (m, 7H, alkyl CH_2), 1.5–1.0 (m, 95H, alkyl-H) 0.85 (t, J = 6.9 Hz, 12H, alkyl CH_3). Anal: calc for $C_{128}H_{152}Cl_2Ga_2N_{16}O_8$ C, 68.24; H, 6.80. Found: C, 69.04; H, 6.15; N, 10.27. UV-vis., λ_{max}/nm (log ε): (THF), 697 (5.37), 619 (4.69), 352 (5.21). MALDI TOF-MS: calculated: 2253.07; found: 2253.97 $[M + 1]^+$.

Tetrakis-4-(hexadecane-1,2-dioxyl)-bis(phthalocyaninato indium(III) chloride) (6). Complex **6** was synthesised in the same manner as **4** by using indium trichloride (0.2 g, 0.90 mmol), yield: 0.21 g (47%), IR (ATR): ν (cm^{-1}): 3063 (Ar–CH), 1623 (C═N/C═C), 1271–1185 (C–O–C). ^{1}H NMR (400 MHz, DMSO) δ 8.68 (dd, J = 8.6, 2.3 Hz, 1H, arom-H), 8.30 (d, J = 8.6 Hz, 1H, arom-H), 7.88 (dt, J = 7.7, 3.8 Hz, 7H, arom-H), 7.62 (dd, J = 24.2, 2.6 Hz, 8H, arom-H), 7.39 (ddd, J = 30.5, 8.8, 2.6 Hz, 7H, arom-H), 5.06 (dd, J = 6.1, 3.5 Hz, 3H, alkyl CH_2/CH), 4.53–4.27 (m, 6H, alkyl CH_2/CH), 2.61 (s, 3H, alkyl-CH_2), 1.97–1.80 (m, 7H, alkyl CH_2), 1.49–1.20 (m, 97H, alkyl CH_2), 0.91 (t, J = 6.6 Hz, 12H, alkyl CH_3). Anal: calc for $C_{128}H_{152}Cl_2In_2N_{16}O_8$ C, 65.61; H, 6.54; Cl, 3.03; In, 9.80; N, 9.56; O, 5.46. Found: C, 66.12; H, 6.82; N, 10.02. UV-vis., λ_{max}/nm (log ε): (THF), 705 (5.14), 642 (4.72), 356 (5.13). MALDI TOF-MS: calculated: 2343.26; found: 2344.02 $[M + 1]^+$.

Fabrication of Pc-polystyrene based thin films. Polystyrene (200 mg) was weighed into clean vials containing 4 mL of chloroform and the mixture was sonicated for 30 min. Then 1×10^{-2} moles each of **4–6** were dissolved in 1 mL of chloroform and transferred into the vials, followed by stirring for 24 h. The homogeneous mixture of Pc-polystyrene was coated on thin glass slides using a Pasteur pipette. The coated glass slides were air dried to remove the chloroform. The resultant thin films are labelled as **4**-PS, **5**-PS, and **6**-PS respectively. The thicknesses of the thin films were determined with the knife edge attachment of a Bruker D8 Discover X-ray diffraction (XRD) system and were found to be 0.015 mm (**4**-PS), 0.021 mm (**5**-PS) and 0.017 mm (**6**-PS).

Results and discussion

Structural characterization

The route for preparation of 4-(hexadecane-1,2-dioxyl)-bis(phthalonitrile) (**3**) and complexes **4–6** is shown in Scheme 1. Complexes **4–6** exhibit varying solubility in different organic solvents, thus making chromatographic purification easier to handle. The disappearance of the sharp C≡N band at 2233 cm^{-1} in the FTIR spectrum of **3**, after cyclotetramerization to form **4–6**, while retaining the aromatic and aliphatic C–H bands between 2952 and 3065 cm^{-1} (for **4–6**) confirms the formation of the respective phthalocyanine complexes.

The C═C and C–O–C vibrations were observed between 1271 and 1115 cm^{-1}. The ^{1}H NMR spectra of **4–6** were similar with only a slight variation in chemical shifts (Fig. S1, ESI†). The spectra showed complex patterns due to the mixed isomer character of these complexes. The aromatic protons from the Pc ring were observed between 8.68 and 7.39 ppm and were integrated to give a total of 24 protons. The long alkyl chain protons resonate from 5 to 1 ppm and were integrated to give a total of 128 protons. The elemental composition and mass spectral data of the complexes corresponded to the expected values. The increased probability of multiple heavy isotopes with an increase in the mass of a molecule causes a decrease in the relative abundance of the monoisotopic peak, hence the isotopic distribution model has been shown to be the accurate method of assigning molecular mass in large molecules[19] such as the one employed in this work. The isotopic mass distribution of the complexes was simulated and compared with the experimental MALDI-TOF measured masses. All the complexes showed fragmentation with a molecular ion peak as $[M + 1]^+$ (Fig. S2, ESI†).

Electronic absorption properties

The main spectral bands in the electronic spectra of **4–6** can be readily assigned to the Q and B bands of Gouterman's 4-orbital model[20] in the 650–750 and 300–400 nm regions, respectively. The shoulder to the red of the B band has been assigned previously to nπ* states associated with the lone pairs of the peripheral oxygen atoms of alkoxy-substituted Pcs,[21] but a destabilization of ππ* states has also been suggested on the basis of TD-DFT calculations.[22] The Q-bands of **4–6** are observed at 682, 697 and 705 nm (Table 1), respectively. A red-shift and broadening are observed in the Q band regions of the ground state electronic absorption spectra of **4–6** (Fig. 1) as the atomic weight of the central metal ion increases.

A strong intermolecular interaction between the Pc rings in ball-type Pc complexes is expected to result in splitting of molecular orbitals and hence lowering of symmetry, resulting in the splitting (or broadening) of the Q band[11] as observed for **5** and **6**. The broadening could also be due to the usual aggregation of phthalocyanines. A further broadening of the spectral bands was observed when the complexes were embedded in polymer thin films. Aggregation of MPc complexes tends to result in two non-vibrational bands at low and high energies, resulting from the monomer and dimer respectively.[23] Aggregation in thin films was judged by red-shifting of the Q band and the presence of high energy peaks at 620, 650 and 655 nm in **4-PS**, **5-PS** and **6-PS** respectively (Fig. 1B). A lack of clear B band peaks is typical of the solid state spectra of phthalocyanines;[24] this could be due to the blue-shifting of all peaks in the solid state. The absorption spectra of **4–6** were recorded at different concentrations in solution. The plots of concentration against absorbance obeyed the Beer–Lambert law confirming non-aggregated species (Fig. 1C, using **5** as example). This confirms that the broadening of the Q band observed for **5** and **6** is not due to aggregation.

MCD spectroscopy and TD-DFT calculations

Analyses of the three Faraday terms, $\mathcal{A}_1$, $\mathcal{B}_0$ and $\mathcal{C}_0$ that form the basis of the theory of MCD spectroscopy provide information on state degeneracies and band polarizations that cannot be derived from the UV-visible absorption spectrum alone.[25]

Table 1 Photophysical data of complexes **4–6** in THF

	λ_{max}	Φ_F	τ_F (ns)	Φ_T	τ_T (μs)	$k_f{}^a$ (s^{-1})	$\tau_{isc}{}^b$ (ns)	k (s)
4	682	0.16	3.28 ± 0.05	0.59	305	4.88×10^7	5.56 ± 0.12	6.87×10^4
5	697	0.08	1.24 ± 0.08	0.73	112	6.45×10^7	1.70 ± 0.16	3.89×10^4
6	705	0.03	0.96 ± 0.03	0.81	74	5.00×10^7	1.19 ± 0.09	1.44×10^4

^{a} $k_f = \frac{\Phi_F}{\tau_f}$ (k_f = fluorescence rate constant). ^{b} $\tau_{isc} = \frac{\tau_F}{\phi_T}$ (τ_{isc} = lifetime for intersystem crossing).

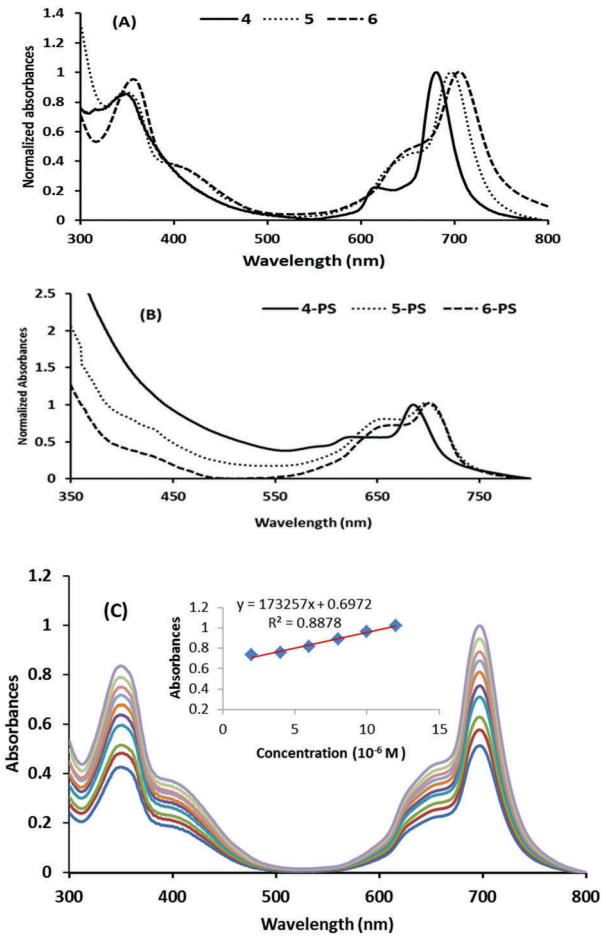

Fig. 1 Absorption spectra of (A) **4**, **5** and **6** in solution, (B) **4**, **5** and **6** in thin films and (C) **5** at different concentrations (inset: Beer–Lambert plot). Solvent: THF.

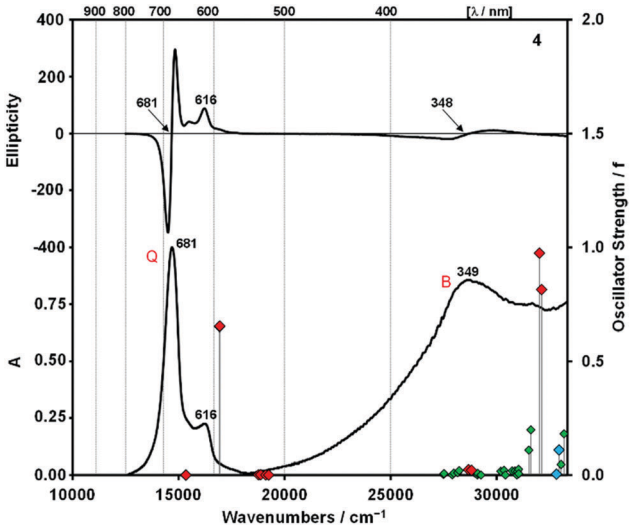

Fig. 2 Absorption and MCD spectra of **4** in THF. The calculated TD-DFT spectrum of the isomer of **4** with four 3,3-position attachments (Fig. S5, ESI†) is plotted against a secondary axis. Red diamonds are used to highlight bands associated with the Q and B bands of Gouterman's 4-orbital model while blue diamonds are used for transitions associated with what would be the $2a_{2u}$ MO of the Pc rings, if D_{4h} symmetry were assumed.

The MCD spectrum of **4** (Fig. 2) is very similar to what would normally be expected for a monomeric ZnPc since pseudo-$\mathcal{A}_1$ terms are observed in the Q and B band regions with cross-over points that correspond to the absorption band maxima[26] This is the pattern that is normally anticipated for dimers with eclipsed rather than staggered structures.[27]

The TD-DFT calculations for **4** (see the ESI† for calculation details) predict single intense bands arising from the Q and B transitions of Gouterman's 4-orbital model[20] in a similar manner to what would be observed for a monomeric $M^{II}Pc$ complex. Similar spectra are predicted for **5** and **6** (Fig. S3 and S4, ESI†) with some minor differences in the B band region, due to the effect of axial chloride ligands on the energy of the $2a_{2u}$ MO of the parent D_{4h} symmetry $M^{II}Pc$ ring. The $1a_{1u}$ and $1e_g{}^*$ frontier MOs of the parent D_{4h} symmetry $M^{II}Pc$ ring combine in bonding and antibonding manners and there is a slight narrowing of the HOMO–LUMO gap for **4–6** (Fig. 3), which accounts for the red shifts that are observed for the Q bands of **5** and **6**.

There is scope for isomerism in the structures of **4–6**, since the point of attachment of the bridging substituent can be at either the 3- or 4-position. Six different structures were calculated for **4**, two with either 3,3- and 3,4-attachments, and four mixed structures arranged in a 3 : 1, oppositely and adjacently arranged 2 : 2, and 1 : 3 manners (Fig. S5, ESI†). Their energies were found to lie within 15 kcal mol^{-1}, so it is reasonable to anticipate that a mixture of these isomers is formed in each case. The calculated TD-DFT spectra are similar enough (Fig. S5 and Table S1, ESI†) that it is reasonable to anticipate a single dominant pseudo-$\mathcal{A}_1$ term in the Q and B band regions. The presence of isomers and the possibility of weak intensity for the forbidden bands that are predicted in the TD-DFT spectra (Fig. 2 and Fig. S3, S4, ESI†) explain the band broadening that is observed in the Q band region relative to the spectra of monomeric $M^{II}Pc$ complexes.[23] It is noteworthy in this regard that although the isomer with only 3,3-position attachments is predicted to be almost perfectly eclipsed, the other isomers are not (Fig. S5, ESI†).

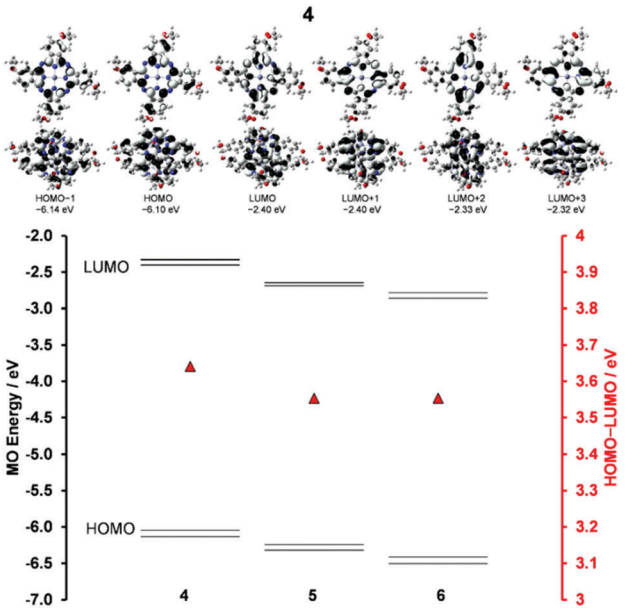

Fig. 3 The angular nodal patterns and energies of the six frontier π-MOs of the isomer of **4** with four 3,3-position attachments (Fig. S5, ESI†) that are associated with the Q transition of Gouterman's 4-orbital model[20] are shown from two perspectives (top). The MO energies and HOMO–LUMO gaps for the isomers of **4–6** with four 3,3-position attachments (bottom). The HOMO–LUMO gaps are highlighted with red diamonds and are plotted against a secondary axis.

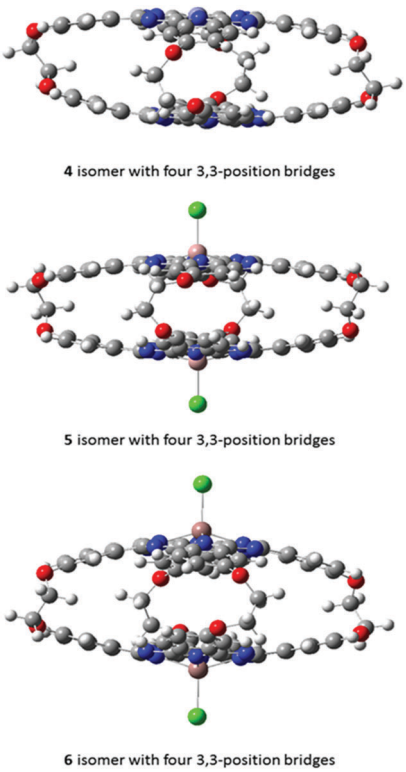

Fig. 4 Side views of the B3LYP optimized geometries of **4–6** for isomers with four 3,3-position bridging moieties.

The optical spectra of **5** and **6** differ somewhat from that of **4** (Fig. 1), because of the presence of axial chloride ligands and the larger Ga(III) and In(III) sitting out of the plane of the Pc π-system (Fig. 4). This leads to significant changes in the vibrational band envelope to the blue of the Q band (Fig. 1), and the differences observed at higher energy in the B band region can be readily explained by the TD-DFT calculations (Fig. 2 and Fig. S3, S4, ESI†), because the axial chloride ligands interact significantly with Pc ring MOs with $1a_{2u}$ and $2a_{2u}$ symmetry (under the D_{4h} symmetry of MPc monomers), since they have large MO coefficients on the pyrrole nitrogen atoms.[28]

Photophysical properties

The emission and excitation spectra of **4** and **6** (as examples) are shown in Fig. 5A and B, respectively. For all complexes, the emission spectra are mirror images of the excitation spectra. For complex **4**, the Q band of the excitation spectrum is slightly red shifted compared to the absorption spectrum, probably due to the different equipment employed for excitation and emission. For complexes **5** and **6**, the excitation spectra no longer show the broadening observed in the absorption spectra.

The fluorescence quantum yields for **5** and **6** are relatively low (Φ_F = 0.08 and 0.03, respectively) when compared to that of **4** (Φ_F = 0.16) (Table 1), which can be attributed to an enhancement of the rate of intersystem crossing by the heavy atom effect. Details of the calculations are provided in the ESI.† The fluorescence lifetimes (τ_F) were obtained by fitting the fluorescence decay data (Fig. 6). A biexponential fit (hence two lifetimes) of

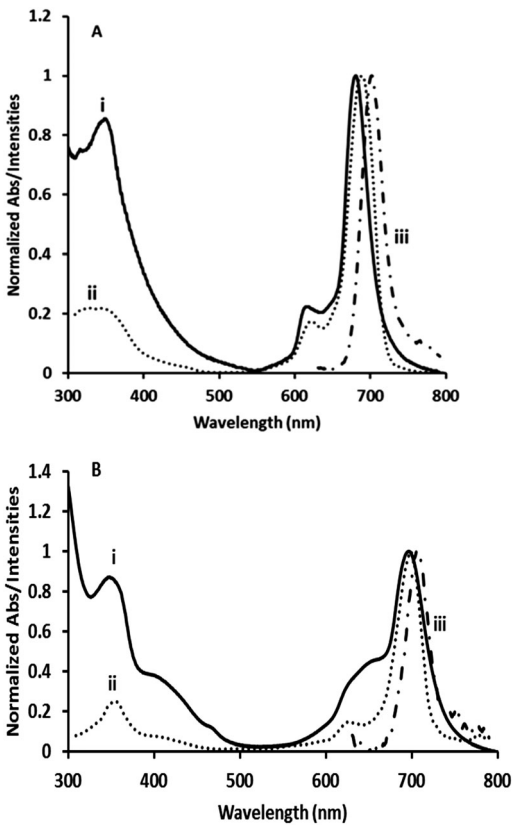

Fig. 5 Absorbance (i), excitation (ii) and emission (iii) spectra of (A) **4** and (B) **6** in THF.

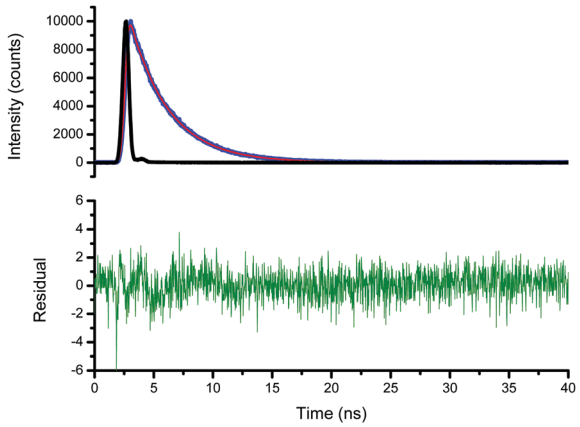

Fig. 6 Fluorescence decay (blue), X^2 fitting (red) and IRF (black) curves of **4** in THF.

3.17 ± 0.08 (22.7%) and 0.32 ± 0.01 ns (77.3%) was obtained for **6** (Fig. S6, ESI†). The average fluorescence lifetime is shown for **6** in Table 1. One lifetime was observed for complexes **4** and **5**. The presence of two lifetimes in Pcs has been reported in terms of the presence of aggregates which quench fluorescence, resulting in quenched (shorter) and unquenched (longer) lifetimes.[29] The fluorescence lifetime is longer for complex **4** compared to complexes **5** and **6**, corresponding to fluorescence quantum yield values. A faster rate of intersystem crossing results in enhanced nonlinear optical properties and a shorter intersystem crossing lifetime. The intersystem crossing lifetimes of the complexes showed that **6** has the lowest value of 1.19 ns while **4** has the longest value. **6** is expected to show enhanced NLO properties as will be discussed below.

An ideal optical limiting material will possess a low fluorescence quantum yield and lifetime, with a high triplet state quantum yield.[30] A typical triplet decay curve is shown in Fig. 7, using complex **4** as an example. The triplet absorption data were fitted to rate eqn (1) in order to determine the triplet lifetime (τ_T)

$$A(t) = A_0 e^{\left(-\frac{t}{\tau_T}\right)} + kt \qquad (1)$$

where $A(t)$ and A_0 are the relative absorbance at time $t = t$ and $t = 0$ respectively; k is the triplet state absorption rate constant

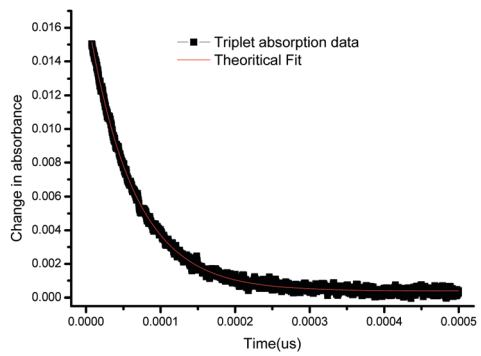

Fig. 7 Triplet absorption decay of complex **4** with the fitting curve. Data were obtained with 3.05 × 10^{-6} M of **4** in THF.

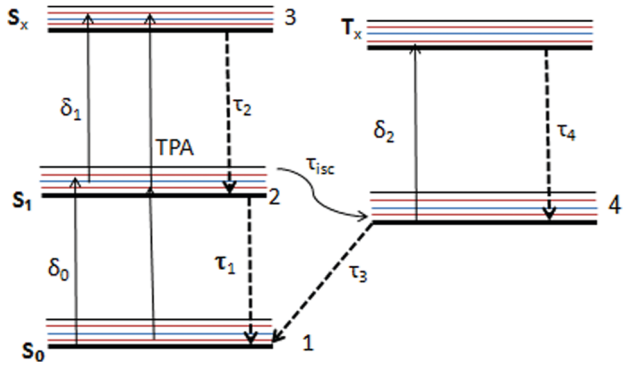

Fig. 8 Energy diagram explaining the dynamics of the excited state population of the complexes.

and τ_T is the triplet excited state lifetime. A best fit to eqn (1) showed triplet lifetimes of 305, 112 and 74 μs, respectively, for **4**, **5** and **6** (Table 1). The corresponding triplet quantum yield values are 0.59, 0.73 and 0.81, respectively. Thus the triplet lifetimes are longer when the triplet quantum yields are smaller as expected.

The corresponding triplet state absorption rate constants (k) were found to be 6.87 × 10^4, 3.89 × 10^4 and 1.44 × 10^4 for **4**–**6**, respectively, which indicate that at every point in time within the irradiation period, 6.87 × 10^4, 3.89 × 10^4 and 1.44 × 10^4 of **4**, **5** and **6**, respectively, are available in the T_1 state (Fig. 8).

This explanation could only be valid with the assumptions that:

(1) All transitions to excited states occur from the ground state, S_0.

(2) The population of the S_1 state is confined by the rate of its deactivation to S_0 or its conversion to the T_1 state through intersystem crossing.

(3) The population of S_n states is negligible ($S_n \approx 0$) since the time-scale of S_n is shorter than the nanosecond pulse duration of the laser.

(4) The intersystem crossing transition from $S_1 \rightarrow T_1$ becomes spontaneous only when the population of S_1 has been saturated.

(5) The $S_1 \rightarrow T_1$ transition is determined by the quantum mechanical condition, $\Delta N = N_t$, where N_t is the number density of excited molecules in the T_1 state per unit time.

With these assumptions in mind, **5** and **6** with $\Delta N = 3.89 \times 10^4$ and 1.44 × 10^4, respectively, will have faster transitions from $T_1 \rightarrow T_n$ than **4** with $\Delta N = 6.87 \times 10^4$ and hence an enhancement of the triplet–triplet absorption transition in the former.[31]

Nonlinear optical (NLO) studies

Reverse saturable absorption. The nonlinear absorption behaviour was measured by using the open aperture Z-scan technique with an excitation pulse of 10 ns at a wavelength of 532 nm and a peak intensity of 360.0 MW cm^{-2}. Reverse saturable absorption (RSA) is one of the main distinguishing features of a suitable nonlinear absorber for optical limiting applications.[32–36] The Z-scan profiles of **4**–**6** exhibit typical RSA signatures (Fig. 9) and the measurements showed NLA behaviours.

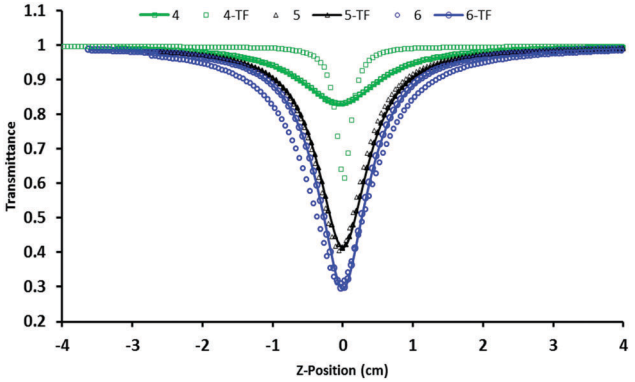

Fig. 9 Nonlinear absorption open-aperture Z-scans for **4–6** in THF and their polymer thin films. A = 1.5, I_{00} = 360 MW cm^{-2}.

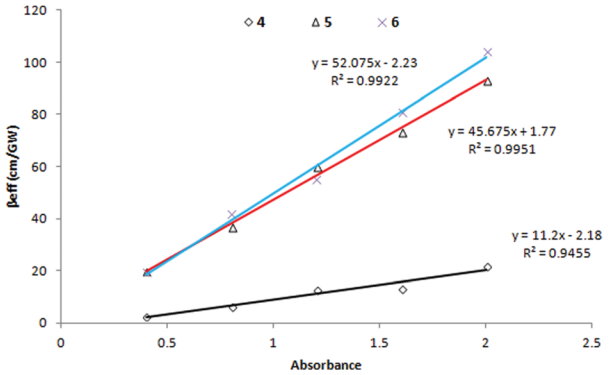

Fig. 10 Plots of absorbance *versus* β_{eff} for **4–6**. Each data point represents an independent Z-scan measurement. $I_{00} \approx$ 360 MW cm^{-2} for each measurement. Solid lines are theoretical fits.

Table 2 Nonlinear optical properties of **4–6** in THF and thin films

		β_{eff} (cm GW^{-1})	$I_m[\chi^3]$ (esu)	γ (esu)	k (δ_{exc}/δ_0)	I_{lim} (J cm^{-2})
4	THF	20.20	4.72×10^{-8}	3.61×10^{-27}	17.72	0.35
	Film	31.30	8.42×10^{-8}	5.68×10^{-27}	28.59	0.23
5	THF	94.20	2.20×10^{-7}	2.50×10^{-26}	57.42	0.11
	Film	95.01	2.56×10^{-7}	2.60×10^{-26}	59.93	0.09
6	THF	105.00	2.45×10^{-7}	2.78×10^{-26}	78.81	0.07
	Film	108.12	2.94×10^{-7}	2.78×10^{-26}	80.35	0.05

The minimum transmittance values were found to drop below 50%, which makes these materials potential candidates for optical limiting applications.[37,38] Table 2 shows the effective nonlinear absorption coefficient values, β_{eff}, which were obtained for each sample by fitting the experimental data to the transmittance equations, eqn (S1)–(S4) (see the ESI† for equations).

It was found that the β_{eff} values increase when the complexes are embedded in polymer thin films (Table 2), but the differences in β_{eff} values between thin films and solutions for **5** and **6** are considerably smaller than that of **4** as can also be seen from Fig. 8. Thin film samples have been reported to exhibit higher photo-degradation thresholds than those in solution. The close NLO response of **5** and **6** both in solution and thin films implies that the two complexes exhibit high photo-stability even in solution. The larger β_{eff} values of **5** and **6** (compared to **4**) correspond to their large triplet quantum yields as a result of the heavy atom effect.

The plot of β_{eff} against absorbance shows the dependence of β_{eff} on the concentration of **4–6** (Fig. 10). It was observed that β_{eff} values increase with the concentration,[39,40] indicating a strong dependence of β_{eff} on the number of available active excited state molecules.

An important measure of a good optical limiting material at 532 nm involves a quantitative evaluation of the ratio of the excited and ground state absorption cross-sections. This is sometimes referred to as the merit coefficient[36] denoted by k. One prerequisite for reverse saturable absorption in optical materials is an excited state absorption cross-section δ_{exc} (δ_1 and δ_2) ($S_1 \rightarrow S_n$ and $T_1 \rightarrow T_n$ transitions) that is larger than the ground state absorption cross-section (δ_0, $S_0 \rightarrow S_1$)[6] (Fig. 8). The occurrence of RSA in complexes **4–6** indicates the existence of an excited state with higher absorption cross-section than the ground state. The excited δ_{exc} values were determined by fitting the data to eqn (S4) (ESI†) and the fit is shown in Fig. S7 (ESI†). This was done in order to determine the dominant mechanism responsible for nonlinearity of each complex at 532 nm and 10 ns pulses.

The ground state absorption cross-sections (δ_0) of the compounds at 532 nm were calculated using an equation described by De Boni *et al.*,[40] eqn (2).

$$\delta_0 = \alpha/N_0 \quad (2)$$

where α is the linear absorption coefficient and N_0 is the number of molecules per cm^3 at 532 nm respectively. The ratios of the excited state cross section to the ground state cross section (k) were evaluated (Table 2). All of the complexes in this study have δ_{exc} values far above those of the ground states (δ_0) by factors ranging from 17.72 to 80.35, both in solution and polymer thin films (Table 2). The population dynamics can be explained using a 5-energy level model (Fig. 8). Depending on the laser pump intensity and wavelength, the absorption mechanism could be (1) transition from the ground state S_0 to the first excited singlet state S_1 and then to the first triplet state T_1 *via* intersystem crossing, (2) direct transition from S_0 to S_n through sequential two photon absorption (TPA), (3) transition from the first excited singlet S_1 to a higher excited state S_n (excited state absorption (ESA)/RSA) or (4) transition from T_1 to T_n states (ESA/RSA). Studies have shown that the nonlinear absorption of phthalocyanines at 532 nm and nanosecond pulse is dominated by ESA/RSA.[31,41,42] In this study, we propose that the mechanism in the observed RSA involves transfer of significant electronic population from the ground singlet state to the lower excited singlet state S_1 or higher excited state S_n. Due to the shorter lifetime of the S_n state, relaxation to S_1 almost occurs immediately and subsequently populates the triplet state *via* intersystem crossing with a lifetime of τ_{isc}. With a high absorption cross-section of the triplet state resulting from high population, most of the incident light will be absorbed leading to a change in transmittance of the laser pulse through the sample in a reverse saturable manner.

Third-order nonlinear susceptibility and second order hyperpolarizability. An important indication of a good optical limiting material is the value of the imaginary component of the third-order nonlinear susceptibility ($I_m[\chi^3]$) since this provides a measure of the speed of the response of an optical material to the perturbation initiated by an intense laser beam.[43] The $I_m[\chi^3]$ values reported in this work (Table 2) are in the order of 10^{-8}–10^{-7} (esu), which are considerably higher than those reported for Pcs and other related macrocycles in solution,[43,44] where values range between $10^{-12}$and 10^{-10}, indicating that these complexes could be good candidates for optical limiting materials.

Upon exposure of a molecule to light, the permanent dipole of the molecule interacts with light which causes a bias in the average orientation of the molecule, resulting in induced hyperpolarizability (γ).

Generally, nonlinear optical properties of a material increase with the γ value. The reported optimal hyperpolarizability values lie in the 10^{-34} to 10^{-29} esu range for Pcs in solution.[43,44] The obtained values of γ in this work (Table 2) lie in the range of 10^{-27} to 10^{-26} which implies that these complexes possess superior nonlinear optical properties. The values of $I_m[\chi^3]$ and γ for **5** and **6** are greater in thin films and in solution than those of **4**, which could be attributed to the presence of heavy atoms in the former.

Optical limiting properties. A good optical limiting (OL) material displays reduced transmittance with increasing incident fluence. This type of device has a linear transmittance at low incident fluence, but abruptly changes at higher incident fluence or there is a threshold at which the output fluence becomes a constant value that should be less than the amount required to damage the optical element.[32,44] This critical point is called the threshold limit intensity or fluence, (I_{lim}),[44,45] which is a very important parameter in optical limiting measurements.

The I_{lim} value may be defined as the input fluence at which the transmittance is 50% of the linear transmittance. Nonlinear optical materials perform better at a low value of I_{lim}. The output–input fluence curves obtained for **5** and **6** (as representatives) in solution and in thin films at 532 nm, 10 ns, and $I_{00} \approx$ 360 MW cm^{-2} are shown in Fig. 11. The red solid line on the plot represents the linear response from which the magnitude of the nonlinearity of the samples is estimated. The complexes exhibit a better performance when embedded in thin films, Table 2, with **6-PS** showing the lowest value of 0.05 (J cm^{-2}), indicating the best optical limiting potential. For the complexes in solution, it was found that **5** and **6** have higher triplet quantum yields than **4** and also have the lowest I_{lim} values, demonstrating the importance of introducing a heavy atom as the central metal ion.

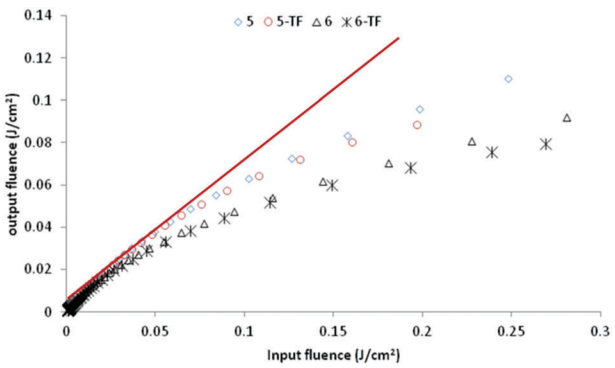

Fig. 11 Output fluence (I_{out}) *versus* input fluence (I_0) curves of **5** and **6** in solution and thin films. Solid lines represent a linear transmission response.

Conclusion

In conclusion, we have synthesised long alkyl ball-type zinc(II), gallium(III) and indium(III) phthalocyanines. The photophysical and nonlinear optical response of the synthesized complexes was evaluated. The Q bands of complexes **5** and **6** containing heavy atoms were more red-shifted compared to that of complex **4**. Low fluorescence quantum yields of 0.08 and 0.03 with the corresponding high triplet quantum yields of 0.73 and 0.81 were also observed for **5** and **6**, respectively. TD-DFT calculations were employed to explain the broadening of the absorption spectra of complexes **5** and **6** as well as the MCD spectra of the complexes. The Z-scan data were fitted taking into account both the nonlinear and excited state absorption processes. All the complexes showed a strong reverse saturable absorption at the excitation wavelength. Complexes **5** and **6** containing heavy atoms were found to give better nonlinear optical response both in solution and when embedded in polymer thin films. Complex **6** bearing indium displayed the best limiting threshold of 0.05 (J cm^{-2}). These results demonstrate that these compounds are good candidates for use in optical limiting applications.

Acknowledgements

This work was supported by the Department of Science and Technology, Republic of South Africa, and the National Research Foundation through DST/NRF South Africa Research Chairs Initiative for Professor of Medicinal Chemistry and Nanotechnology (Grant number UID 62620) and Rhodes University.

Notes and references

1 X.-L. Zhang, X. Zhao, Z.-B. Liu, S. Shi, W.-Y. Zhou, J.-G. Tian, Y.-F. Xu and Y.-S. Chen, *J. Opt.*, 2013, **13**, 7–11.
2 T. Chervy, J. Xu, Y. Duan, C. Wang, L. Mager, M. Frerejean, J. A. W. Münninghoff, P. Tinnemans, J. A. Hutchison, C. Genet, A. E. Rowan, T. Rasing and T. W. Ebbesen, *Nano Lett.*, 2016, **16**, 7352–7356.
3 G. Torre, P. Vázquez, F. Agulló-López and T. Torres, *Chem. Rev.*, 2004, **104**(9), 3723–3750.
4 M. O. Senge, M. Fazekas, E. G. A. Notaras, W. J. Blau, M. Zawadzka, O. B. Locos and E. M. Ni Mhuircheartaigh, *Adv. Mater.*, 2007, **19**, 2737–2774.
5 M. de Torres, S. Semin, L. Razdolski, J. Xu, J. A. A. W. Elemans, T. Rasing, A. E. Rowan and R. J. M. Nolte, *Chem. Commun.*, 2015, **51**, 2855–2858.

6 J. Xu, S. Semin, T. Rasing and A. E. Rowan, *Small*, 2015, **11**, 1113–1129.
7 S. Varghese, M. Iype, E. J. Mathew and C. S. Menon, *Mater. Lett.*, 2002, **56**, 1078–1083.
8 T. Yamada, H. Hoshi, T. Manaka, K. Ishikawa, H. Takezoe and A. Fukuda, *Phys. Rev. B: Condens. Matter Mater. Phys.*, 1996, **53**, R13314.
9 J. Wang and W. J. Blau, *J. Opt. A: Pure Appl. Opt.*, 2009, **11**, 024001.
10 Z. Li and W. Sun, *Dalton Trans.*, 2013, **42**, 14021–14029.
11 Z. Odabaş, A. Altindal, A. R. Özkaya, M. Bulut, B. Salih and Ö. Bekaroğlu, *Polyhedron*, 2007, **26**, 695–707.
12 M. A. Özdağ, T. Ceyhan, H. Ünver, A. Elmali and Ö. Bekaroğlu, *Opt. Commun.*, 2010, **283**, 330–334.
13 L. De Boni, L. Gaffo, L. Misoguti and C. R. Mendonça, *Chem. Phys. Lett.*, 2006, **419**, 417–420.
14 S. V. Rao, P. T. Anusha, L. Giribabu and S. P. Tewari, *J. Phys.*, 2010, **75**(5), 1017–1023.
15 K. Sanusi and T. Nyokong, *J. Photochem. Photobiol., A*, 2015, **303–304**, 44–52.
16 S. D'Souza, E. Antunes, C. Litwinski and T. Nyokong, *J. Photochem. Photobiol., A*, 2011, **220**, 11–19.
17 S. B. Piepho and P. N. Schatz, *Group Theory in Spectroscopy with Applications to Magnetic Circular Dichroism*, Wiley-VCH Verlag GmbH, New York, 1983.
18 K. E. Sekhosana and T. Nyokong, *Opt. Mater.*, 2015, **47**, 211–218.
19 N. Srinivasan, C. A. Haney, J. S. Lindsey, W. Zhang and B. Chait, *J. Porphyrins Phthalocyanines*, 1999, **3**, 283–291.
20 M. Gouterman, in *Optical Spectra and Electronic Structure of Porphyrins and Related Rings. In The Porphyrins*, ed. D. Dolphin, Academic Press, New York, 1978, vol. III, Part A, pp. 1–165.
21 Z. Gasyna, N. Kobayashi and M. J. Stillman, *J. Chem. Soc., Dalton Trans.*, 1989, 2397–2405.
22 J. Mack, N. Kobayashi and M. J. Stillman, *J. Inorg. Biochem.*, 2010, **102**, 472–479.
23 M. J. Stillman and T. Nyokong, in *Phthalocyanine. Principles and Properties*, ed. C. C. Leznoff and A. B. P. Lever, VCH Publications, New York, 1989, vol. 1, pp. 133–290.
24 L. Alagna, A. Capobianchi, M. P. Casaletto, G. Mattogno, A. M. Paoletti, G. Pennesi and G. Rossi, *J. Mater. Chem.*, 2001, **11**, 1928–1935.
25 E. Glimsdal, M. Carlsson, T. Kindahl, M. Lindgren, C. Lopes and B. Eliasson, *J. Phys. Chem. A*, 2010, **114**, 3431–3442.
26 T. Nyokong, Z. Gasyna and M. J. Stillman, *Inorg. Chem.*, 1987, **26**, 1087–1095.
27 J. Kleinwächter and M. Hanack, *J. Am. Chem. Soc.*, 1997, **119**, 10684–10695.
28 J. Mack, J. Stone and T. Nyokong, *J. Porphyrins Phthalocyanines*, 2014, **18**, 630–641.
29 Z. Petrásek and D. Phillips, *Photochem. Photobiol. Sci.*, 2003, **2**, 236–244.
30 K. Sanusi, J. M. Stone and T. Nyokong, *New J. Chem.*, 2015, **39**, 1665–1677.
31 Y. Chen, M. Hanack, W. J. Blau, D. Dini, Y. Liu, Y. Lin and J. Bai, *J. Mater. Sci.*, 2006, **41**, 2169–2185.
32 M. Hanack, T. Schneider, M. Barthel, J. S. Shirk, S. R. Flom and R. G. S. Pong, *Coord. Chem. Rev.*, 2001, **219–221**, 235–258.
33 Y. Chen, L. R. Subramanian, M. Fujitsuka, O. Ito, S. O. Flaherty, W. J. Blau, T. Schneider, D. Dini and M. Hanack, *Chemistry*, 2002, **8**(18), 4248–4254.
34 Y. Chen, L. Gao, M. Feng, L. Gu, N. He, J. Wang, Y. Araki, W. J. Blau and O. Ito, *Mini-Rev. Org. Chem.*, 2009, **6**, 55–65.
35 M. Hanack, D. Dini, M. Barthel and S. Vagin, *Chem. Rec.*, 2002, **2**, 129–148.
36 Y. Chen, Y. Araki, M. Fujitsuka, M. Hanack, O. Ito, S. M. O'Flaherty and W. J. Blau, *Solid State Commun.*, 2004, **131**, 773–778.
37 P. K. Hegde, A. V. Adhikari, M. G. Manjunatha, P. Poornesh and G. Umesh, *Opt. Mater.*, 2009, **31**, 1000–1006.
38 K. Sanusi, E. K. Amuhaya and T. Nyokong, *J. Phys. Chem. C*, 2014, **118**, 7057–7069.
39 K. Sanusi, E. Antunes and T. Nyokong, *Dalton Trans.*, 2014, **43**, 999–1010.
40 L. De Boni, L. Gaffo, L. Misoguti and C. R. Mendonça, *Chem. Phys. Lett.*, 2006, **419**, 417–420.
41 A. B. Karpo, V. E. Pushkarev, V. I. Krasovskii and L. G. Tomilova, *Chem. Phys. Lett.*, 2012, **554**, 155–158.
42 M. Yüksek, A. Elmali, M. Durmuş, H. Gul Yaglioglu, H. Ünver and T. Nyokong, *J. Opt.*, 2010, **12**, 015208.
43 R. L. Sutherland, D. G. Mclean and S. Kirkpatrick, *Handbook of Nonlinear Optics with contributions by*, Mercel Dekker INC, New York, 2nd edn, 2003.
44 *The Porphyrin Handbook Phthalocyanines: Properties and Materials*, ed. R. Guilard, K. Kadish and K. M. Smith, Academic Press, New York, 2003.
45 C. P. Singh, K. S. Bindra, B. Jain and S. M. Oak, *Opt. Commun.*, 2005, **245**, 407–414.

